Available online at www.sciencedirect.com

SciVerse ScienceDirect

Energy Procedia 16 (2012) 1526 – 1534

Energy Procedia

2012 International Conference on Future Energy, Environment, and Materials

Dynamic Characteristic Analysis of Doubly-fed Induction Generator Low Voltage Ride-through

L. Shi, N. Chen and Q. Lu

Abstract

For studying the impacts of wind turbines integrated into grid, the relation between the protection of doubly-fed induction generator (DFIG) during low voltage fault and the dynamic characteristic of grid is established from the points of generator operation constrains and district grid voltage stability. Then the resistance value and switching strategy of crowbar are discussed. Based on analyzing the electric characteristic of the voltage or current during the short-circuit fault in wind turbines with crowbar switching, the equation to estimate peak current of stator and rotor of DFIG with crowbar switching and the value range of crowbar resistance are derived. The numeric test analyzes the impacts of crowbar switching on district grid voltage stability with different fault types, crowbar switching time and crowbar resistance values. Also the interaction impact of crowbar switching on multi-wind farms is analyzed. The results show that reasonable crowbar resistance value and switching strategy can improve low voltage ride through (LVRT) ability of wind turbines and reduce bad impacts on district grid voltage stability with large-scale crowbar switching of wind farms.

Keywords: Low voltage ride through (LVRT); doubly fed induction generator (DFIG); crowbar; voltage stability.

1. Introduction

With large scale wind power integrated into grid, its impacts on gird stability has been an important issue. Now, more and more grid operators required that wind turbines must have LVRT ability [1]-[3].

Manuscript received Aug 10, 2010. This work was supported in part by Key Project of the National Eleventh-Five Year Research Program of China under Grant 2008BAA14B04.

Lei Shi is with the State Grid Electric Power Research Institute, sub-branch of State Grid Corporation of China, Nanjing 210003, Jiangsu Province, China, phone:86-25-83098031; fax:86-25-83098130; e-mail: shilei@sgepri.sgcc.com.cn.

Ning Chen is with the State Grid Electric Power Research Institute, sub-branch of State Grid Corporation of China, Nanjing 210003, Jiangsu Province, China, phone:86-25-83098031; fax:86-25-83098025; e-mail: chenning8375@163.com.

Qiang Lu is with the State Grid Electric Power Research Institute, sub-branch of State Grid Corporation of China, Nanjing 210003, Jiangsu Province, China, e-mail: luqiang@sgepri.sgcc.com.cn.

 doi:10.1016/j.egypro.2012.01.239

DFIG stator links with grid directly, so grid voltage sags will cause terminal voltage sags and rotor over-current which may damage generator and converter [4]. It is difficult to realize LVRT [5]-[6]. However, additional crowbar circuit provides a method. Crowbar resistance value selection has been studied in [7]-[9]. Physical process of DFIG LVRT has been studied in [7] and [10].

In fact, DFIG LVRT and grid impact with each other when grid voltage sags. LVRT control can make DFIG maintain connection with grid so that DFIG can supply reactive power to support grid voltage. But long duration will make DFIG absorb reactive power from grid.

From the point of mutual impacts between DFIG LVRT and grid, dynamic characteristic of DFIG LVRT will be studied in this paper. The analysis of short-circuit current is described in Section II, the analysis of LVRT characteristic in SectionⅢ, and the numerical analysis in Section IV. Finally, the conclusions are drawn in Section V.

2. Analysis of Short-circuit Current

2.1 Equivalent Model of DFIG

Equivalent model of DFIG is shown in Fig.1.

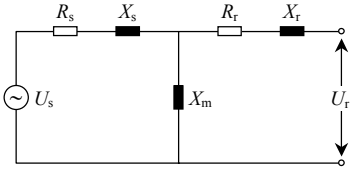

Fig. 1 Equivalent model of DFIG .

Rotor orientation method is used to analysis generator dynamic characteristic, so electromagnetic transient model is described as

$$\begin{cases} U_{ds} = \mathrm{D}\psi_{ds} - \omega_r \psi_{qs} + r_s I_{ds} \\ U_{qs} = \mathrm{D}\psi_{qs} + \omega_r \psi_{ds} + r_s I_{qs} \\ U_{dr} = \mathrm{D}\psi_{dr} + r_r I_{dr} \\ U_{qr} = \mathrm{D}\psi_{qr} + r_r I_{qr} \end{cases} \tag{1}$$

$$\begin{cases} \psi_{dr} = X_{rr} I_{dr} + X_m I_{ds} \\ \psi_{qr} = X_{rr} I_{qr} + X_m I_{qs} \\ \psi_{ds} = X_{ss} I_{ds} + X_m I_{dr} \\ \psi_{qs} = X_{ss} I_{qs} + X_m I_{qr} \end{cases} \tag{2}$$

Where, r_s is stator resistance, x_s is stator leakage reactance, r_r is rotor resistance, x_r is rotor leakage reactance, U_{ds} is stator voltage in d-axis, U_{qs} is stator voltage in q-axis, U_{dr} is rotor voltage in d-axis, U_{qr} is rotor voltage in q-axis, I_{ds} is stator current in d-axis, I_{qs} is stator current in q-axis, I_{dr} is rotor current in d-axis, I_{qr} is rotor current in q-axis, ψ_{ds} is stator flux in d-axis, ψ_{qs} is rotor flux in q-axis, ψ_{dr} is rotor flux in d-axis, ψ_{qr} is rotor flux in q-axis, ω_r is rotor angular velocity, X_m is excitation reactance, $X_{rr} = X_m + x_r$, $X_{ss} = X_m + x_s$, D is differential operator.

Considering transient flux change, the relation among rotor current, rotor voltage and stator current is

derived from equation (1) and (2),

$$\begin{cases} I_{dr} = \dfrac{U_{dr} - \mathrm{D}X_{\mathrm{m}} I_{ds}}{\mathrm{D}X_{\mathrm{rr}} + r_{\mathrm{r}}} \\ I_{qr} = \dfrac{U_{qr} - \mathrm{D}X_{\mathrm{m}} I_{qs}}{\mathrm{D}X_{\mathrm{rr}} + r_{\mathrm{r}}} \end{cases} \tag{3}$$

The relation among stator flux, rotor voltage and stator current is derived form eqution (2) and (3),

$$\begin{cases} \psi_{ds} = \dfrac{X_{\mathrm{m}}}{\mathrm{D}X_{\mathrm{rr}} + r_{\mathrm{r}}} U_{dr} + (X_{\mathrm{ss}} - \dfrac{\mathrm{D}X_{\mathrm{m}}^2}{\mathrm{D}X_{\mathrm{rr}} + r_{\mathrm{r}}}) I_{ds} \\ \psi_{qs} = \dfrac{X_{\mathrm{m}}}{\mathrm{D}X_{\mathrm{rr}} + r_{\mathrm{r}}} U_{qr} + (X_{\mathrm{ss}} - \dfrac{\mathrm{D}X_{\mathrm{m}}^2}{\mathrm{D}X_{\mathrm{rr}} + r_{\mathrm{r}}}) I_{qs} \end{cases} \tag{4}$$

Assuming $G(\mathrm{D}) = X_{\mathrm{m}}/(\mathrm{D}X_{\mathrm{rr}}+r_{\mathrm{r}})$, $X(\mathrm{D}) = X_{\mathrm{ss}} - \mathrm{D}X_{\mathrm{m}}^2/(\mathrm{D}X_{\mathrm{rr}}+r_{\mathrm{r}})$, stator voltage is described as

$$\begin{cases} U_{ds} = \mathrm{D}[G(\mathrm{D})U_{dr} + X(\mathrm{D})i_{ds}] - \\ \qquad \omega_{\mathrm{r}}[G(\mathrm{D})U_{qr} + X(\mathrm{D})i_{qs}] + r_{\mathrm{s}} i_{ds} \\ U_{qs} = \mathrm{D}[G(\mathrm{D})U_{qr} + X(\mathrm{D})i_{qs}] + \\ \qquad \omega_{\mathrm{r}}[G(\mathrm{D})U_{dr} + X(\mathrm{D})i_{ds}] + r_{\mathrm{s}} i_{qs} \end{cases} \tag{5}$$

$$\dot{U}_{\mathrm{s}} = (\mathrm{D} + \mathrm{j}\omega_{\mathrm{r}})(G(\mathrm{D})\dot{U}_{\mathrm{r}} + X(\mathrm{D})\dot{I}_{\mathrm{s}}) + r_{\mathrm{s}}\dot{I}_{\mathrm{s}} \tag{6}$$

In the rotor orientation coordination, stator steady-state voltage is described as

$$\begin{cases} U_d = U \sin(-s\omega_0 t + \delta) \\ U_q = U \cos(-s\omega_0 t + \delta) \end{cases} \tag{7}$$

2.2 Analysis of Stator Current Characteristic

Usually, the maximum short-circuit current appears when three –phases fault occurs at generator terminal. Then rotor time constant T_{r} and stator time constant T_{s} are defined as

In power flow calculation, common modified equation is generally defined as

$$\begin{cases} T_{\mathrm{s}} = X_{\mathrm{ss}} / r_{\mathrm{s}} \\ T_{\mathrm{r}} = X_{\mathrm{rr}} / (r_{\mathrm{r}} + R_{\mathrm{crowbar}}) \end{cases} \tag{8}$$

Where, R_{crowbar} is crowbar reactance.

According to equation (6), stator current can be described as

$$\dot{I}_{\mathrm{s}} = \dot{U}_{\mathrm{s}} / [x(\mathrm{D})(\mathrm{D} + \mathrm{j}\omega_{\mathrm{r}} + r_{\mathrm{s}} / x(\mathrm{D}))] \tag{9}$$

Because $X_{\mathrm{rr}} >> r_{\mathrm{r}}$, equation (10) is described as

$$\frac{r_{\mathrm{s}}}{x(\mathrm{D})} = \frac{r_{\mathrm{s}}}{X_{\mathrm{ss}}(\mathrm{D}\sigma X_{\mathrm{rr}} + r_{\mathrm{r}})/(\mathrm{D}X_{\mathrm{rr}} + r_{\mathrm{r}})} \approx \frac{r_{\mathrm{s}}}{\sigma X_{\mathrm{ss}}} = \frac{1}{\sigma T_{\mathrm{s}}} \tag{10}$$

Then equation (9) can be described as

$$\dot{I}_{\mathrm{s}} = \frac{\dot{U}_{\mathrm{s}}}{x(\mathrm{D})[\mathrm{D} + \mathrm{j}\omega_{\mathrm{r}} + 1/(\sigma T_{\mathrm{s}})]} \tag{11}$$

According to Hay Computing，equation (11) can be described as

$$\dot{I}_{\mathrm{s}} = \frac{U\mathrm{e}^{\mathrm{j}s\omega_0 t-\mathrm{j}\delta-90^\circ}}{x(\mathrm{D})[\mathrm{D}+\mathrm{j}\omega_{\mathrm{r}}+1/(\sigma T_{\mathrm{s}})]} = \frac{U\mathrm{e}^{-\mathrm{j}\delta-90^\circ}\mathrm{e}^{\mathrm{j}s\omega_0 t}}{x(\mathrm{D}+\mathrm{j}s\omega_0)[\mathrm{D}+\mathrm{j}s\omega_0+\mathrm{j}\omega_{\mathrm{r}}+1/(\sigma T_{\mathrm{s}})]} \tag{12}$$

Then equation (13) is derived,

$$\dot{I}_{\mathrm{s}} = \sqrt{\frac{(s\omega_0 T_{\mathrm{r}})^2+1}{(s\omega_0\sigma T_{\mathrm{r}})^2+1}}\frac{U\mathrm{e}^{\mathrm{j}\varphi_0}}{\sigma\omega_0 X_{\mathrm{ss}}}\{\frac{1/(\sigma T_{\mathrm{r}})-1/T_{\mathrm{r}}+\mathrm{j}\omega_{\mathrm{r}}}{1/(\sigma T_{\mathrm{s}})-1/(\sigma T_{\mathrm{r}})+\mathrm{j}\omega_{\mathrm{r}}}\cdot \mathrm{e}^{-t/(\sigma T_{\mathrm{s}})}+[1/T_{\mathrm{r}}-1/(\sigma T_{\mathrm{r}})][\frac{1}{1/(\sigma T_{\mathrm{r}})+\mathrm{j}s\omega_0}+\frac{1}{1/(\sigma T_{\mathrm{s}})-1/(\sigma T_{\mathrm{r}})+\mathrm{j}\omega_{\mathrm{r}}}]e^{-t/(\sigma T_{\mathrm{r}})+\mathrm{j}\omega_{\mathrm{r}}t}\} \tag{13}$$

Where, $\sigma=1-X_{\mathrm{m}}^2/(X_{\mathrm{rr}}X_{\mathrm{ss}})$, is MFL coefficient.

,Because$\omega_{\mathrm{r}}>>1/(\sigma T_{\mathrm{s}})-1/(\sigma T_{\mathrm{r}})$, equation (14) is derived approximatively,

$$I_{\mathrm{s}} \approx \frac{U\sqrt{1+1/(2\pi\sigma)^2}}{\sigma\omega_0 X_{\mathrm{ss}}}\cdot [(\sigma-1)\mathrm{e}^{-t/(\sigma T_{\mathrm{r}})+\mathrm{j}(\omega_{\mathrm{r}}t+\varphi_0+\delta)}+\mathrm{e}^{-t/(\sigma T_{\mathrm{s}})+\mathrm{j}(\varphi_0+\delta)}] \tag{14}$$

$$\delta=\arctan[1/(\sigma T_{\mathrm{r}}\omega_{\mathrm{r}})] \tag{15}$$

Assuming $\alpha=\varphi_0+\delta$, equation (17) is described as

$$\mathrm{Re}(I_{\mathrm{s}}) \approx \frac{U\sqrt{1+1/(2\pi\sigma)^2}}{\sigma\omega_0 X_{\mathrm{ss}}}\cdot [(\sigma-1)\mathrm{e}^{-t/(\sigma T_{\mathrm{r}})}\cos(\omega_{\mathrm{r}}t+\alpha)+\mathrm{e}^{-t/(\sigma T_{\mathrm{s}})}\cos\alpha] \tag{16}$$

Then equation (17) and (18)is derived from equation (14) and (16),

$$\frac{\partial\,\mathrm{Re}(I_{\mathrm{s}})}{\partial t} = \frac{U\sqrt{1+1/(2\pi\sigma)^2}}{\sigma\omega_0 X_{\mathrm{ss}}}[\frac{(1-\sigma)}{\sigma T_{\mathrm{r}}}\mathrm{e}^{-t/(\sigma T_{\mathrm{r}})}\cdot \cos(\omega_{\mathrm{r}}t+\alpha)+(1-\sigma)\omega_{\mathrm{r}}\mathrm{e}^{-t/(\sigma T_{\mathrm{r}})}\sin(\omega_{\mathrm{r}}t+\alpha)- 1/(\sigma T_{\mathrm{s}})\mathrm{e}^{-t/(\sigma T_{\mathrm{s}})}\sin\alpha] = 0 \tag{17}$$

$$\frac{\partial\,\mathrm{Re}(I_{\mathrm{s}})}{\partial\alpha} = \frac{U\sqrt{1+1/(2\pi\sigma)^2}}{\sigma\omega_0 X_{\mathrm{ss}}}[(1-\sigma)\mathrm{e}^{-t/(\sigma T_{\mathrm{r}})}\cdot \sin(\omega_{\mathrm{r}}t+\alpha)-\mathrm{e}^{-t/(\sigma T_{\mathrm{s}})}\sin\alpha]=0 \tag{18}$$

Known by equation (17) and (18), the extremum appears when angle α and time t meet equation (19) and (20),

$$\alpha = 0 \tag{19}$$

$$t = T_r/2 \tag{20}$$

So the extremum of stator short-circuit current is described as,

$$I_{s,em} \approx \frac{U\sqrt{1+1/(2\pi\sigma)^2}}{\sigma\omega_0 X_{ss}}[(1-\sigma)e^{-1/(2\sigma)} + e^{-T_r/(2\sigma T_s)}] \tag{21}$$

2.3 Analysis of Rotor Current Characteristic

Because electromagnetic transient process is short when crowbar switching, DFIG operation in asynchronous state and rotor current can be described as

$$I_r = \frac{-DX_m}{DX_{rr} + r_r} I_s \tag{22}$$

Then maximum rotor current at T/2 can be derived from equation (23) approximatively,

$$I_{rmax} \approx X_m I_s / X_{ss} \tag{23}$$

Known by equation (24), rotor current has the similar attenuation law with stator current, and its value is smaller than stator current. Its reason is that transient process of crowbar switching is ignored. In order to make result approaching the actual value, rotor current is as

$$I_{rmax} \approx I_s \tag{24}$$

3. Analysis of LVRT Characteristic

3.1 Crowbar reactance value selection

Known by equation (21) and (24), U_{max} is a function relation to $R_{crowbar}$, as $U_{max}=f(R_{crowbar})$. Then equation (25) is derived as

$$f = \frac{U_s X_{rr}}{X_{ss}\sqrt{1+(\omega_r\sigma T_r)^2}} \cdot \{\frac{\omega_r\sigma T_r X_{rr}}{[1+(\omega_r\sigma T_r)^2]R_{cr}^2} - \frac{T_m}{\sigma X_{rr}}\}e^{-T_m/(\sigma T_r)} + \frac{U_s X_{rr}\omega_r\sigma T_r X_{rr}}{X_{ss}[1+(\omega_r\sigma T_r)^2]^{3/2} R_{cr}^2} e^{-T_m/(\sigma T_s)} \tag{25}$$

Usually, the value equation (25) is above 0, so maximum rotor voltage monotonically increases with crowbar reactance value increase after crowbar switching. Fig.2 shows the result comparison with calculation and simulation of the relation between U_{max} and crowbar reactance value.

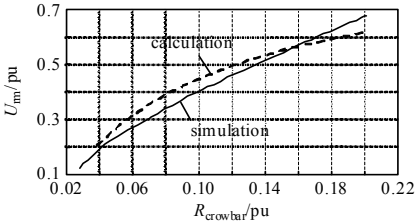

Fig. 2 Result comparison with calculation and simulation .

Assuming maximum rotor voltage during fault is described as

$$U_{\mathrm{rmax}} = I_{\mathrm{rmax}} R_{\mathrm{crowbar}} \tag{26}$$

Where, I_{rmax} is maximum rotor current.

To avoid over-voltage at rotor side, safety margin coefficient λ is set, so upper limit of crowbar reactance value is selection according to

$$R_{\mathrm{crowbar}} = U_{\mathrm{rmax}}/I_{\mathrm{rmax}} < \lambda U_{\mathrm{rlim}}/I_{\mathrm{rmax}} \tag{27}$$

Where, U_{rlim} is rotor voltage limit。

Additionally, DFIG operates in asynchronous state and absorb reactive power from grid during voltage recovering period. If crowbar reactance value is too small, it will cause over-current again. So crowbar reactance value should be selected according to grid characteristic.

3.2 Crowbar switching strategy

Wind power is concentrated integrated into high voltage grid in China, so that it strengthens the coupling of wind farms. If converter can recover control mode timely after transient process ending during fault, it can balance active power and support grid voltage to improve grid stability. Otherwise, it will extend the transient process. So the time for recovering converter control should be set as 20~40ms after fault clearing, in order to avoid.

4. Numerical Analysis

4.1 Test System Introduction

The test system is an actual grid with three integrated wind farms, one plant and two constant power loads, shown in Fig.3. Where, plant volume is 500MW, load1 volume is 220MW/30MVar, load2 volume is 300MW/180Mvar, WF1 and WF2 volume are 100MW, WF3 volume is 50MW. All wind farms are integrated into grid by 220kV transmission lines.

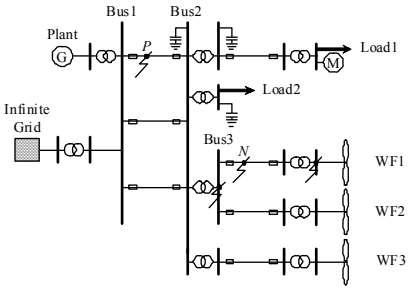

Fig. 3 Test system.

4.2 LVRT Analysis in Different Conditions

Assuming three different faults as
Fault1: Terminal of WF1 occurs three-phases short circuit fault at 0s;
Fault2: Point N occurs three-phases short circuit fault at 0s;
Fault3: Point P occurs three-phases short circuit fault at 0s.
Simulation results are shown in Fig.4 and Fig.5.

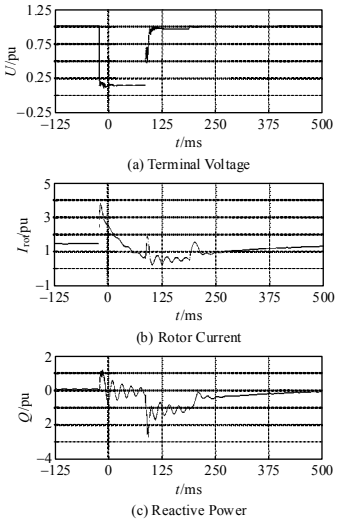

Fig. 4 LVRT characteristic when short circuit occurs at WF1 erminal.

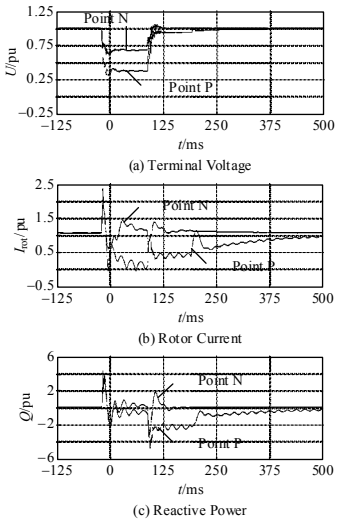

Fig. 5 LVRT characteristic when short circuit occurs at Line.

From Fig.4-a and Fig.5-a, it is seen that when fault occurs, WF1 terminal voltage sags to 0.2p.u. in fault1, 0.4p.u. in fault2 and 0.7p.u. in fault3. So we can conclude that it has larger impacts on wind farm with closer electrical distance. From Fig.4-b and Fig.5-b, it is seen that rotor current is up to 4.5p.u. in fault1, larger than fault2 and fault3, so we can conclude that it is easier to realize LVRT with farther electrical distance. From

Fig.4-c and Fig.5-c, it is seen that DFIG generates reactive power when fault occurs, but absorbs reactive power after fault clearing until crowbar switch. Summing up, the transient process is the same with equation (21).

4.3 LVRT Analysis in Different Switching Time

Assuming that short circuit fault occurs at WF1 terminal at 0s, then the fault is cleared at 100ms, crowbar switch time is set as 80ms, 100ms, 120ms and 200ms respectively. LVRT characteristics in four different switching time are analyzed, the simulation result is shown in Fig.6.

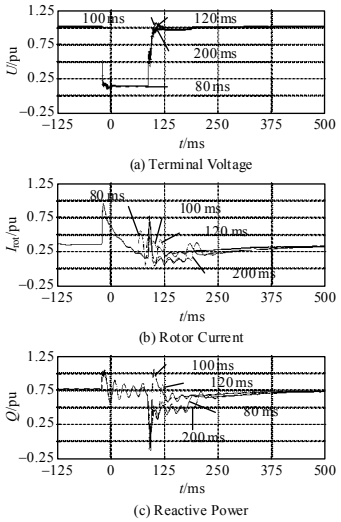

Fig. 6 LVRT characteristic in different crowbar switching time.

From Fig.6-b and Fig.6-c, it is seen that if crowbar switching time is 80ms, a new transient process causes rotor over-current to make crowbar switch again and DFIG absorb reactive power from grid before fault clearing. If crowbar switching time is 200ms, a new transient process causes rotor over-current to make crowbar switch again and DFIG absorb reactive power from grid after fault clearing. If crowbar switching time is 100ms, coinciding witch fault clearing time, the transient process caused by fault clearing will plus with that caused by crowbar switching so that maximum current is up to 3p.u. and absorbed reactive power up to 3.5p.u.. If crowbar switching time is 120ms, the transient process caused by crowbar switching lags behind that caused by fault clearing. Its maximum current is 1.7p.u. and absorbed reactive power is 2.4p.u..

Summing up, crowbar switching time is an important index for LVRT control， inappropriate crowbar switching time is not conducive to grid voltage recovering.

5. Conclusion

Stator and rotor short-circuit current expressions which are applying on engineering to estimate their values are analyzed. Based on this, the criterion to select crowbar reactance value and the time to switch crowbar are proposed. The result of numerical test shows that appropriate crowbar reactance value and switching time can improve LVRT control characteristic and grid stability.

References

[1] Abbey C, Joos G, “Effectoflow voltage ride through (LVRT) characteristic on voltage stability”, IEEE Trans. on Industry Applications, vol.41, No.3, pp.1-7, 2005.

[2] Xie Bing, Fox B, Flynn D, “Study of fault ride-through for DFIG wind turbines”, IEEE Intenraitonla Conference on Electric Uitlity Deregulaiton Restructuring and Power Technolclgies, Hong Kong, China, 2004.

[3] Morren J, Sjoerd W H, “Ride through of wind turbines with doubly-fed induction generator during a voltage dip”, IEEE Trans. on Energy Conversion, vol.20, No.2, pp.435-441, 2005.

[4] Yao Jun, Liao Yong, Tang Jianping, “Ride-through control strategy of AC excited wind-power generator for grid short-circuit fault”, Proceedings of the CSEE, vol.27, No.30, pp.64-71, 2007.

[5] Li Yu, Guan Hongliang, Zhao Haifeng, et al, “LVRT capability of wind turbine generator and its application to regional power grid”, Proceedings of 5th World Wind Energy Conference, Delhi, India, 2006.

[6] Wang Wei, Sun Mingdong, Zhu Xiaodong, “Analysis on the low voltage ride through of DFIG”, Automation of Electric Power Systems, vol.31, No.23, pp.84-89, 2007.

[7] Morren J, Haan S W H, “Ride-through of wind turbines with doubly-fed induction generator during a voltage dip”, IEEE Trans. on Energy Convers, vol.20, No.2, pp.435-442, 2005.

[8] Niiranen J, “Voltage dip ride through of doubly-fed generator equippedwith active Crowbar”, The Nordic Wind Power Conference, Gothen-burg, Sweden, 2004.

[9] Perdana A, Carlson O, Persson J, “Dynamic response of grid-connected wind turbine with doubly fed induction generator during disturbances”, Nordic Workshop on Power and Industrial Electronics, Trondheim, Norway, 2004.

[10] Morren J, Haan S W H, “Short-circuit current of wind turbines with doubly fed induction generator”, IEEE Trans. on Energy Conversion, vol.22, No.1, pp.174-180, 2007.

[11] Hu Jiabing, Sun Dan, He Yikang, et al, “Modeling and control of DFIG wind energy generation system under grid voltage dip”, Automation of Electric Power Systems, vol.30, No.8, pp.21-26, 2006.

[12] Li Jing, Song Jiahua, Wang Weisheng, “Modeling and dynamic simulation of variable speed wind turbine with large capacity”, Proceedings of the CSEE, vol.24, No.6, pp.100-105, 2004.